ON THE USE OF A MIXED MULTISCALE FINITE ELEMENT METHOD FOR GREATER FLEXIBILITY AND INCREASED SPEED OR IMPROVED ACCURACY IN RESERVOIR SIMULATION

JØRG E. AARNES, SINTEF APPLIED MATHEMATICS*

Abstract. In this paper we propose a modified mixed multiscale finite element method for solving elliptic problems with rough coefficients arising in e.g., porous media flow. The method is based on the construction of special base functions which adapt to the local property of the differential operator. In particular the method incorporates the effect of small scale heterogeneous structures in the elliptic coefficients into the base functions and produces a detailed velocity field that can be used to solve phase transport equations at a subgrid-scale. The method is mass conservative and accounts for radial flow in the near-well region without resorting to complicated well models or near-well upscaling procedures. As such, the method provides a step toward a more accurate and rigorous treatment of advanced well architectures in reservoir simulation. The accuracy of the method is demonstrated through a series of 3D incompressible two-phase flow simulations.

Key words. two-phase flow, porous media, multiscale methods, reservoir simulation

AMS subject classifications. 76Txx, 76S05, 74Sxx, 81T80

The accuracy of reservoir simulation is largely controlled by the geological grid models. The need to capture fine-scale heterogeneities has lead to an intensive research on 3D seismic, petrophysical and geological modeling. State-of-the-art reservoir characterization methods based on stochastic methods now allow for generation of a large number of plausible high-resolution grid models, each consisting of multi-million cells. Similarly, the need to represent large-scale structures like channels and faults or complex trajectories of deviated, multi-branch wells require models with complex geometries. This has been reflected in complex gridding schemes like Voronoi grids, corner-point-grids, locally refined grids, flow-based grids, etc. On top of this, increased demands for history matching and uncertainty assessment require fast and accurate flow simulations on multiple plausible geological models on a routinely basis.

Commercial reservoir simulators have not kept up with this development and there is a gap of orders of magnitude between the size of the geological grid models and the size of the grid models used in routine reservoir simulation. Reservoir simulators have therefore relied on upscaling procedures, [9, 14, 22, 24, 25, 26], that reduce the level of detail to a manageable amount of data. However, although upscaling is of widespread use, it has many potential pitfalls, see e.g. [3], and must be used with great care since fine-scale details have a strong impact on the overall flow pattern. This is even more true for near-well upscaling procedures, [13, 15], since it is vital that we capture the effect of the heterogeneous structures in the vicinity of the wells in order to produce reliable production scenarios.

Several multiscale methods, [11, 19, 20], have recently been promoted as a robust alternative to upscaling. In these new mathematical methods, fine-scale heterogeneous features are incorporated at a subgrid scale through the design of appropriate "coarse scale" approximation spaces. Accurate velocity fields can later be reconstructed on a finer subgrid from the coarse grid solution, hence without mesh refinement. This allows us to include more of the geological data into the numerical model and to treat the wells at a much smaller scale than what is possible with monoscale numerical

*Corresponding address: SINTEF Anvendt Matematikk, PB. 124, Blindern, N-0314 Oslo, Norway. Email: Jorg.Aarnes@sintef.no. Phone: + 47 22 06 77 95. Fax: + 47 22 06 73 50.

schemes. We shall use the term multiscale solution to denote a fine grid solution that has been reconstructed from the coarse grid solution.

Even though the multiscale methods have only begun to find applications outside of academia, we believe that they are now at a stage where they can be promoted to the industry. It is our belief that multiscale methods will be gradually acknowledged, not as a complex numerical tool for applications with special needs, but as a flexible numerical tool that is easy to adapt to complex real world applications. Among the many reasons for this belief, we mention:

- *Multiscale methods allow great flexibility in the design of the simulation grid and does not confine the shape of the grid blocks as the standard finite element methods or finite difference methods do.*
- *Multiscale methods allows us to adapt the subgrid to small scale features such as fractures, faults and high permeability streaks, and thus also assign to local regions specially tuned parameters.*
- *Multiscale methods are ideally suited for local grid refinement strategies since the subgrid "velocity" field is implicitly contained in the multiscale solution and hence can be recovered whenever it is needed in the simulation.*
- *Multiscale methods are well suited for parallel computing environments since the multiscale base functions can be computed independently.*

In the multiscale FEM (MsFEM) that was introduced by Hou and Wu, [19], one attempts to capture the small-scale influence through base functions constructed from special numerical greens functions. Actually this method was a generalization of the "generalized FEM's" developed by Babuška and Osborn, [1, 2], but Hou and Wu were the first to acknowledge their potential to solve elliptic problems with rough coefficients in multiple dimensions. They also showed (in 2D) that for elliptic problems with periodic coefficients, the multiscale solution converges to the correct homogenized solution as the scale of periodicity tends to zero.

In this paper we develop a variant of the mixed MsFEM proposed by Chen and Hou, [11]. Unlike the original MsFEM [19], the mixed MsFEM produces a globally (but not necessarily locally) mass conservative velocity field and is therefore better suited for problems describing transport phenomena. Another mass conservative multiscale method is the multiscale finite volume method (MsFVM) developed by Jenny et al, [20]. This method is based on the finite volume methodology which is popular in reservoir simulation communities, but it still requires the construction of special multiscale base functions. Moreover, in our opinion it is a bit more cumbersome to construct a fine grid velocity field for the MsFVM than it is for the mixed MsFEM.

The objective with this study has been to modify the mixed MsFEM so that it generates a velocity field that is mass conservative both globally and locally (inside the coarse grid elements) so that it can be used to simulate two-phase flow at the subgrid scale. The motivation for doing this is that the elliptic part of a two-phase flow simulation usually stands for the majority of the CPU time. Hence, by using the mixed MsFEM to solve the elliptic pressure equation at the "coarse scale" level and a fast numerical scheme, e.g. a streamline method, [4, 6, 23], to solve the phase transport equation at the subgrid level, we can achieve a speedup of several orders of magnitude compared with traditional monoscale reservoir simulation schemes.

In this study we have not made any attempt to optimize the computing time. Instead we have focused on modifying the existing mixed MsFEM of Chen and Hou, [11], and made an effort to show that it produces a velocity field with accuracy comparable to that of a reference solution obtained by solving the elliptic pressure equation at the fine-scale level. To this end we have compared simulated water-cut curves, i.e. the fraction of water in the produced fluid, rather than the velocity fields themselves which are somewhat less informative. This is because a velocity field that is globally similar to the true solution may still produce very poor production scenarios if it fails to identify the high flow regions correctly.

The paper is organized as follows. We present the mathematical model governing immiscible incompressible two-phase flow in section 1, and derive the global pressure - total velocity formulation from the Darcy law and the continuity equation. We then explain what is meant by *multiscale methods* in section 2, and introduce the mixed MsFEM by Chen and Hou, [11]. We use this method as a reference when we make the modifications that lead to the multiscale method that we study in this paper. In section 3 we include a brief description of the upstream weighted finite volume method that we use to solve the phase transport equations. In section 4 we do a series of numerical experiments. We here show that the proposed mixed MsFEM can be used to obtain high accuracy at a low cost and identify situations where the mixed MsFEM must be applied with care. Finally, we make some concluding remarks and give some suggestions for further work.

1. The mathematical two-phase flow model. The differential equations that model immiscible and incompressible two-phase flow can be derived from the Darcy law, describing the relation between the phase pressure p_i and the phase velocity v_i,

$$v_i = -K\lambda_i(\nabla p_i - \rho_i G) \ , \tag{1.1}$$

and the corresponding continuity equation

$$\phi\frac{\partial S_i}{\partial t} + \nabla\cdot v_i = q_i \ . \tag{1.2}$$

Here the saturations S_i denote the fraction of the accessible void volume of the porous medium filled by the respective phases and q_i is a source term representing wells. We shall assume that the phases are oil (o) and water (w) and that the two phases together fill the void space completely so that $S_o + S_w = 1$. Furthermore, K is the rock permeability tensor assumed to be symmetric and uniformly positive definite

$$0 < \alpha \le \xi^T K(x)\xi \le \beta \qquad \forall\xi\in\mathcal{R}^d\ , \forall x\in\Omega\ ,$$

and $\lambda_i = \frac{k_{ri}}{\mu_i}$ is the phase mobility where k_{ri} and μ_i are the relative permeability and viscosity of phase i. Typical relative permeability curves for an oil-water system are shown in Figure 1.1. Finally ρ_i, ϕ and $G = -(0,0,g)^T$ denote respectively the phase density, the porosity and the gravity acceleration vector where g is the gravitational constant. Moreover, for simplicity we let $q = q_w + q_o$ and introduce the total mobility $\lambda_t = \lambda_w + \lambda_o$, the fractional flow function $f_i = \lambda_i/\lambda_t$, the gravitational mobility $\lambda_g = \lambda_w\rho_w + \lambda_o\rho_o$, the total filtration velocity $v = v_w + v_o$ and the capillary pressure $p_{cow} = p_o - p_w$, assumed to be a given function that only depends on the saturation.

If we now sum the Darcy equations (1.1) for oil and water we derive

$$v = -K\lambda_t(\nabla p_o - f_w\nabla p_{cow}) + K\lambda_g G\ . \tag{1.3}$$

Invoking the total differential condition, i.e., we assume that there exists a function $p_c = p_c(S_w)$ such that $\nabla p_c = f_w\nabla p_{cow}$, then we obtain an an elliptic equation for the global pressure $p = p_o - p_c$:

$$v = -K(\lambda_t\nabla p - \lambda_g G) \qquad \text{and} \qquad \nabla\cdot v = q\ . \tag{1.4}$$

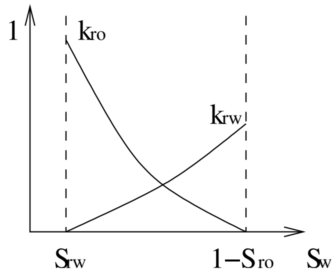

FIG. 1.1. *Typical relative permeability curves for an oil-water system.*

If p_c exists then it is easy to show that p_c is given by

$$p_c(S_w) = \int_1^{S_w} f_w(\xi)\frac{\partial p_{cow}}{\partial S_w}(\xi)d\xi \ .$$

Finally we use (1.2) to derive a mass transport equation for e.g., the water phase. Expanding $\nabla p_{cow} = \frac{\partial p_{cow}}{\partial S_w}\nabla S_w$ and using simple algebraic manipulations we deduce

$$v_w = f_w(v + K\lambda_o\frac{\partial p_{cow}}{\partial S_w}\nabla S_w + K\lambda_o(\rho_w - \rho_o)G) \ . \tag{1.5}$$

Since our main focus in this paper is on numerical methods for the elliptic pressure equation, we shall use a simple upstream weighted finite volume method to solve the saturation equation. This implies that the numerical diffusion can dominate the diffusive effects from capillary forces. Thus, in order not to produce ambiguous results we neglect effects from capillary forces. Hence, the final form of the saturation equation that will be used to compute the phase transport becomes

$$\phi\frac{\partial S_w}{\partial t} + \nabla\cdot f_w\,(v + K\lambda_o(\rho_w - \rho_o)G) = q_w \ . \tag{1.6}$$

However, we wish to emphasize that the mixed MsFEM method that we propose below can be coupled with any available numerical method for solving the saturation equation since it provides explicit fluxes at the cell interfaces.

2. Multiscale methods for elliptic problems in porous media flow. The heterogeneous porous media formations in oil-reservoirs typically lead to rock permeability tensors K that vary rapidly over short distances. This rapidly oscillatory behavior creates some fundamental problems with respect to designing robust reservoir simulation schemes. In particular, it is well known that details at all spatial length scales may have a strong impact on the global flow conditions. Furthermore, the impact of the fine scale heterogeneous structures on the global flow behavior is non-trivial and simple averaging routines are found to be inadequate. We therefore need to develop methods that integrate the fine scale information into the coarse scale equations in a way which is consistent with the local property of the differential operator. This is the basic idea behind the construction of a multiscale method.

The oldest, and most widely known multiscale method for elliptic problems is the homogenization method, [18, 21]. The homogenization theory has evolved into a rich mathematical theory which identifies the elliptic operators that arise in the limit of a sequence of elliptic operators with periodic coefficients as the scale of periodicity tends to zero. As such it has few direct applications, but it has provided valuable insight into how small-scale heterogeneous features affect the corresponding elliptic solution. In the context of porous media flow, homogenization has been used to obtain equivalent grid-block permeability. The idea here is to consider each grid block as a periodic cell in an infinite heterogeneous media. Under these circumstances, the effective, or equivalent permeability of each block can be approximated by the respective homogenized tensors. The concept of homogenization is hence used as an upscaling procedure and aims at quantifying the macroscopic behavior of the flow.

The idea behind the recent multiscale numerical methods, [11, 19, 20], is somewhat different. Instead of seeking upscaled effective parameters, the methods attempt to construct low dimensional approximation spaces that are sensitive to the fine scale variations in the elliptic coefficients. In this way, these multiscale methods not only attempt to capture the large scale trends in the flow process, but also the important fine scale characteristics. Unfortunately it is not trivial to analyze these multiscale methods, but convergence results have been obtained for the MsFEM's, [11, 19], using results from the homogenization theory. These convergence estimates are thus strictly valid only for periodic structures, but the MsFEM's themselves are not limited to elliptic problems with periodic coefficients. In fact, numerical experience shows that they perform well for a wide range of heterogeneous fine-scale formations.

2.1. The mixed multiscale finite element method. Denote the reservoir domain by $\Omega \subset \mathcal{R}^d$, let n be the outward pointing unit normal on $\partial\Omega$ and define

$$H_0^{1,div}(\Omega) = \{q \in (L^2(\Omega))^d : \nabla \cdot q \in L^2(\Omega),\ q \cdot n = 0 \text{ on } \partial\Omega\}\ .$$

Then the mixed formulation of (1.4) reads: find $(p, v) \in L^2(\Omega) \times H_0^{1,div}(\Omega)$ such that

$$\int_\Omega (K\lambda_t)^{-1} v \cdot u\ dx - \int_\Omega p\ \nabla \cdot u\ dx = \int_\Omega (f_w\rho_w + f_o\rho_o) G \cdot u\ dx \tag{2.1}$$

$$\int_\Omega l\ \nabla \cdot v\ dx = \int_\Omega ql\ dx, \tag{2.2}$$

for all $u \in H_0^{1,div}(\Omega)$ and $l \in L^2(\Omega)$. For a discretization of (2.1)-(2.2) to be successful, there must be a balance between the approximation space for the pressure p and the Darcy velocity v. One possibility is to choose $V \subset H_0^{1,div}(\Omega)$ and $U \subset L^2(\Omega)$ so that $U = div(V)$. This follows from the Ladyzhenskaya-Babuška-Brezzi theory; see e.g., [8], or any standard textbook on finite element methods such as [5] or [7].

In the original version of the mixed MsFEM (MMsFEM) that was introduced by Chen and Hou, [11], one seeks a solution to the mixed problem (2.1)-(2.2) in a finite dimensional subspace $(U, V^{ms}) \subset L^2(\Omega) \times H_0^{1,div}(\Omega)$. The multiscale aspect comes from the fact that V^{ms} is spanned by base functions that reflect the impact of the local heterogeneous structures on the differential operator. The base functions for the MMsFEM [11] are defined as follows.

Let $\mathcal{K} = \{K\}$ be a partitioning of Ω into polyhedral elements and denote the set of interfaces by $\{\Gamma_{ij} = \partial K_i \cap \partial K_j\}$. For each interface Γ_{ij} we associate a base function $\psi_{ij} = -K\lambda_t\nabla\phi_{ij}$ where ϕ_{ij} is defined by

$$\nabla \cdot \psi_{ij} = |K_i|^{-1} \text{ in } K_i, \quad \text{and} \quad \nabla \cdot \psi_{ij} = -|K_j|^{-1} \text{ in } K_j\ , \tag{2.3}$$

subject to e.g., the compatible boundary conditions

$$\psi_{ij} \cdot n_{ij} = |\Gamma_{ij}|^{-1} \text{ on } \Gamma_{ij}, \quad \text{and} \quad \psi_{ij} \cdot n = 0 \text{ on } \partial K_i \cup \partial K_j \backslash \Gamma_{ij}\ . \tag{2.4}$$

Here n_{ij} is the coordinate unit normal to Γ_{ij} pointing from K_i to K_j and n is the outward unit normal on $\partial(K_i \cup \Gamma_{ij} \cup K_j)$. We then define $V^{ms} = span\{\psi_{ij} : \Gamma_{ij} \neq \emptyset\}$. Observe that the base functions are defined so that each $v \in V^{ms}$ is continuous in the direction of the unit normal n_{ij} at the interface Γ_{ij}. Hence, $V^{ms} \subset H_0^{1,div}(\Omega)$ and $div(V^{ms}) = \mathcal{P}_0(\mathcal{K})$. The corresponding MMsFEM therefore seeks $(p, v) \in U \times V^{ms}$ with $U = \mathcal{P}_0(\mathcal{K})$ that satisfy (2.1)-(2.2) for all $u \in V^{ms}$ and $l \in U$.

The subgrid problems (2.3)-(2.4) may be solved with any suitable numerical method, not necessarily a FEM. However, if a finite difference or finite volume method is applied, then we need to map the corresponding solution onto an appropriate function space which allows us to compute the cross-terms $[\int_\Omega (K\lambda_t)^{-1}\psi_{ij} \cdot \psi_{kl}]$. The subgrid may be chosen to model physical features such as fractures and faults, or to be tuned to advanced well architectures. Moreover, the MMsFEM does not restrict the geometry of the grid blocks, nor does it require that the subgrids in neighboring blocks have matching grid lines at the interface. See figure 1.1 for an illustration.

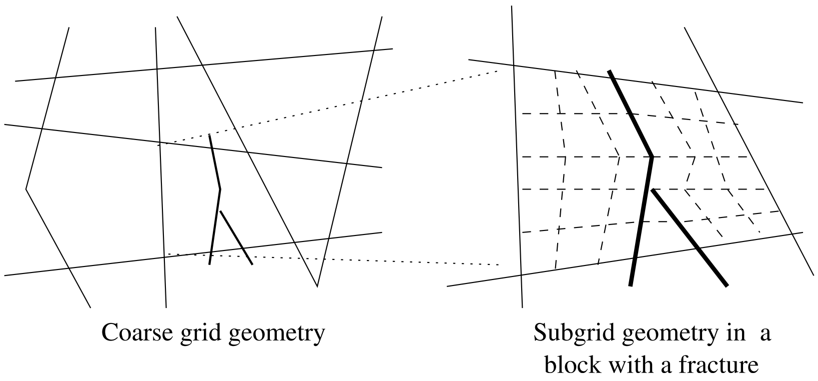

FIG. 2.1. *Examples of possible grid structures that involve complicated geometries which may be difficult to handle with conventional numerical methods.*

2.2. A modified mixed multiscale FEM for fast reservoir simulation. The MMsFEM introduced by Chen and Hou, [11], needs to be modified if we want to use the resulting velocity field to simulate the phase transport at a subgrid-scale. This is because the constant local source terms in (2.3) produce a velocity field that does not preserve mass inside the well blocks. Indeed, the constant source terms for the base functions in (2.3) imply that the subgrid velocity field induced by the MMsFEM of Chen and Hou would only be locally mass conservative inside the well blocks if the wells are treated as a uniform source that is smeared out over the whole block. We therefore propose a slightly different variant of the MMsFEM where the base functions $\psi_{ij} = -K\lambda_t\nabla\phi_{ij}$ satisfy

$$(\nabla \cdot \psi_{ij})|_{K_i} = \begin{cases} 1/|K_i| & \text{if } \int_{K_i} f\,dx = 0 \\ f/\int_{K_i} f\,dx & \text{else ,} \end{cases} \tag{2.5}$$

$$(\nabla \cdot \psi_{ij})|_{K_j} = \begin{cases} -1/|K_j| & \text{if } \int_{K_j} f\,dx = 0 \\ -f/\int_{K_j} f\,dx & \text{else ,} \end{cases} \tag{2.6}$$

and are subject to some boundary conditions

$$\psi_{ij} \cdot n = 0 \;\text{ on } \partial K_i \cup \partial K_j \backslash \Gamma_{ij} \quad \text{and} \quad \psi_{ij} \cdot n_{ij} = \nu_{ij} \;\text{ on } \Gamma_{ij}\,. \tag{2.7}$$

Here ν_{ij} is a boundary condition with $\int_{\Gamma_{ij}} \nu_{ij}\, ds = 1$ that will be specified in §2.3.

We observe that this definition still guarantees that $\psi_{ij} \cdot n_{ij}$ is continuous across the interface Γ_{ij} ($\psi_{ij} \cdot n_{kl}$ is clearly continuous across all other interfaces). It follows that $V^{ms} \subset H_0^{1,div}(\Omega)$, but, unfortunately, it is no longer true that $div(V^{ms}) = \mathcal{P}_0(\mathcal{K})$. This observation indicates that we might also have to alter the approximation space for the pressure variable. Indeed, the alternative definition of the base functions in (2.5)-(2.6) implies that the induced MMsFEM is particularly sensitive to the pressure at the wells. The space $U = \mathcal{P}_0(\mathcal{K})$ is not rich enough to account for the difference between the pressure at the wells and the average pressure in the well blocks.

Thus, to define a new approximation space for the pressure p we assume that $(p, v) \in L^2(\Omega) \times H_0^{1,div}(\Omega)$ satisfies (2.1)-(2.2) for all $l \in \mathcal{P}_0(\mathcal{T})$ and $u \in V^{ms}$ and write $p = \bar{p} + \hat{p}$ where and $\hat{p}$ has zero average over all $T \in \mathcal{T}$. Then $\int_T \hat{p}\ \nabla \cdot u\ dx$ vanishes everywhere except in the well blocks. Hence, if $\hat{p}$ solves

$$\int_T \hat{p} = 0, \qquad \hat{v} = -K(\lambda_t \nabla \hat{p} - \lambda_g G), \qquad \nabla \cdot \hat{v} = q, \qquad \hat{v} \cdot n = \nu_T, \tag{2.8}$$

in the well blocks for some appropriate compatible boundary conditions ν_T on ∂T and vanishes elsewhere, then $\hat{U} = \hat{p} + \mathcal{P}_0(\mathcal{T})$ defines an approximation space that correctly accounts for the difference the pressure at the wells and the average pressure in the well blocks. We therefore propose to solve (1.4) with the mixed FEM which seeks $v^{ms} \in V^{ms}$ and $p \in \hat{U}$ such that (2.1)-(2.2) holds for all $u \in V^{ms}$ and $l \in \mathcal{P}_0(\mathcal{T})$.

Remark: It is usually enough to regenerate a small portion of the base functions at each time step since the total mobility λ_t only varies significantly in the vicinity of the propagating saturation front. We propose to regenerate a base function ψ_{ij} if

$$\int_{T_i} \lambda_t(S_w)\, dx \qquad \text{or} \qquad \int_{T_j} \lambda_t(S_w)\, dx \tag{2.9}$$

has changed more than some threshold C since the previous update. This criteria is a bit crude, but it should perform well as long as we specify a sensible threshold value.

Thus, if we decide not to regenerate a particular set of base functions, then we use the corresponding base functions from the previous time step together with the recently updated ones. This means that the "old" base functions will not satisfy (2.5)-(2.6) unless the mobility in K_i and K_j has changed with a constant multiple. This introduces an improper relative weighting of the elliptic coefficients in the base functions, but it does not destroy the subgrid mass balance.

2.3. The selection of boundary conditions. We now propose two different strategies that can be used to determine the local boundary conditions ν_{ij} and ν_T in (2.7) and (2.8). We first use a deterministic approach and define boundary conditions for the base functions ψ_{ij}. These boundary conditions determine the possible inter-block flow conditions induced by the numerical solution $v^{ms} \in V^{ms}$. They should therefore reflect the heterogeneous structures at the interfaces Γ_{ij} and account for a radial flow pattern in the near-well region.

If we are away from the near-well region, then it is reasonable to assume uniform direction of flow so that $v \cdot n_{ij}$ is constant and proportional to $\upsilon_{ij} := n_{ij} \cdot K\lambda_t n_{ij}$ on Γ_{ij}. This observation promotes the following boundary conditions:

$$\nu_{ij}(x) = \frac{\upsilon_{ij}(x)}{\int_{\Gamma_{ij}} \upsilon_{ij}(s)\, ds}\ , \quad x \in \Gamma_{ij}\ . \tag{2.10}$$

To define boundary conditions in the near-well region we first assume that we have a singular source term at $x_i \in T$ and uniform radial flow. Then the radial flow velocity at $x \in \Gamma_{ij}$ must scale proportional to $dist(x, x_i)^{1-d}$ in order to preserve mass. If a well-block contains more than one well, or the well has a finite perforation length, then the radial flow velocity at $x \in \Gamma_{ij}$ should scale according to the total contribution from all sources. Combining this observation with the impact of local heterogeneous structures suggest the following boundary conditions for a well-block interface:

$$\nu_{ij}(x) = \frac{w(x)\upsilon_{ij}(x)}{\int_{\Gamma_{ij}} w(s)\upsilon_{ij}(s)\, ds}\ , \quad \text{where} \quad w(x) = \int_T q(\xi)|x-\xi|^{1-d}\, d\xi\ , \quad x \in \Gamma_{ij}. \tag{2.11}$$

Here we have assumed that all well rates are specified. If they are determined by the bottom-hole pressure, then we first need to use e.g., a Peaceman type well model at the subgrid scale in order to specify corresponding well rates.

Though the role of $\hat{p}$, to account for the difference between the pressure at the wells and the average pressure in the corresponding well-block, is different from the role of the base functions ψ_{ij}, we use the same considerations to obtain local boundary conditions for $\hat{p}$ as we did to obtain the boundary conditions ν_{ij} associated with a well block interface. Hence, assume that $q|_T \neq 0$ and define $\upsilon_T = n_T \cdot K\lambda_t n_T$ on ∂T where n_T the outward pointing unit normal on ∂T. Then the boundary conditions for $\hat{p}$ that correspond to the boundary conditions (2.11) for ψ_{ij} are defined by

$$\nu_T(x) = w(x)\upsilon_T(x)\frac{\int_T q(\xi)\, d\xi}{\int_{\partial T} w(s)\upsilon_T(s)\, ds}\ , \qquad x \in \partial T\ . \tag{2.12}$$

The boundary conditions (2.10)-(2.12) take into account features that have a local effect on the flow, but does not incorporate flow properties caused by e.g., the global boundary conditions. This kind of information is difficult to incorporate unless we know something about the global flow pattern. However, for multi-phase flow applications one can sometimes justify the computation of the initial velocity field v^0 on a fine grid. If we assume that we can afford to compute v^0 on a fine grid, then we can define more robust boundary conditions ν_{ij} and ν_T for $t > t_0$ according to

$$\nu_{ij}(x,t) = \frac{\lambda_t(x,t)}{\lambda_t(x,t_0)}(v^0 \cdot n_{ij}) \qquad x \in \Gamma_{ij},\ t > t_0\ , \tag{2.13}$$

$$\nu_T(x,t) = \frac{\lambda_t(x,t)}{\lambda_t(x,t_0)}(v^0 \cdot n_T) \qquad x \in \partial T,\ t > t_0\ . \tag{2.14}$$

Observe that if v^0 and the base functions (2.5)-(2.6) are computed on the same grid with a mixed FEM, then the multiscale solution $v \in V^{ms}$ induced by (2.13)-(2.14) at $t = t_0$ coincides with v^0.

Figure 2.2 displays base functions for a two dimensional model with homogeneous coefficients using the boundary conditions (2.10) and (2.11). The two plots in top row of Figure 2.2 correspond to an interface away form the near well region. This base function is identical to the corresponding base function for the Raviart-Thomas mixed FEM of lowest order on regular quadrilateral grids. The base function depicted in the bottom row of Figure 2.2 correspond to a well-block interface. The delta-like peak seen in the x-component corresponds to the well location. We note that the interface is hardly visible in these plots. This demonstrates that the radial distance weighting in (2.11) accounts for the radial flow pattern in a proper way.

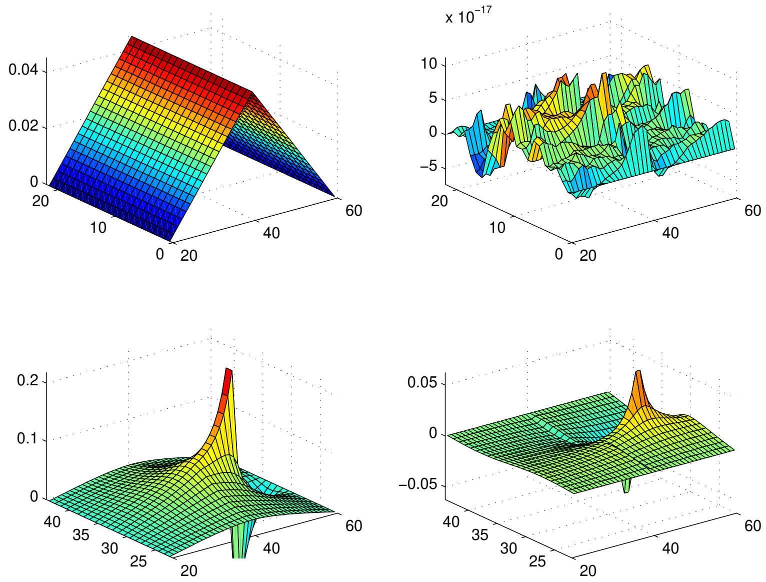

FIG. 2.2. *The x-component (left) and y-component (right) of two MMsFEM base functions for a two dimensional model with homogeneous coefficients. The top base function corresponds to an interface away from the near well region and is constructed using (2.10) while the bottom base function corresponds to a well block interface and is constructed using (2.11).*

Figure 2.3 displays the corresponding base functions for a two dimensional model with random coefficients, i.e., the coefficients are selected at random from the interval $(0, 1)$. Thus, in addition to the radial distance weighting in (2.11) we also scale the flux at across the interface according to (2.10). The plots in Figure 2.3 demonstrate that the MMsFEM base functions are highly sensitive to the fine scale details in the heterogeneous formation and thus creates an approximation space for the velocity which reflects the fine scale characteristics in the geological model.

2.4. Some remarks on the novelty of the modified MMsFEM. The most significant new feature in the modified MMsFEM, as compared with the original MMsFEM of Chen and Hou, is that we use non-constant source terms in the equations that define the base functions in the well blocks. The reason for doing this is that we want the multiscale solution to be both globally and locally mass conservative so that the induced velocity field can be used to simulate the phase transport at the subgrid level. This adjustment has two important implications. First of all we need to add a correction term to the discretized equations that account for the large gradients in the well-blocks. Secondly we can not use an oversampling strategy to define the boundary conditions since this would cause us to loose the mass balance property at the element interfaces. We have therefore suggested two alternative strategies for specifying the boundary conditions for the base functions:

- *A "static" approach where we at each time step define boundary conditions that reflect the heterogeneous structures at the interfaces and the configuration of the wells in the near well region.*
- *A dynamic approach where we compute the initial velocity field v^0 on a fine grid and use information about the global flow pattern to update the boundary conditions for the base functions at subsequent time steps.*

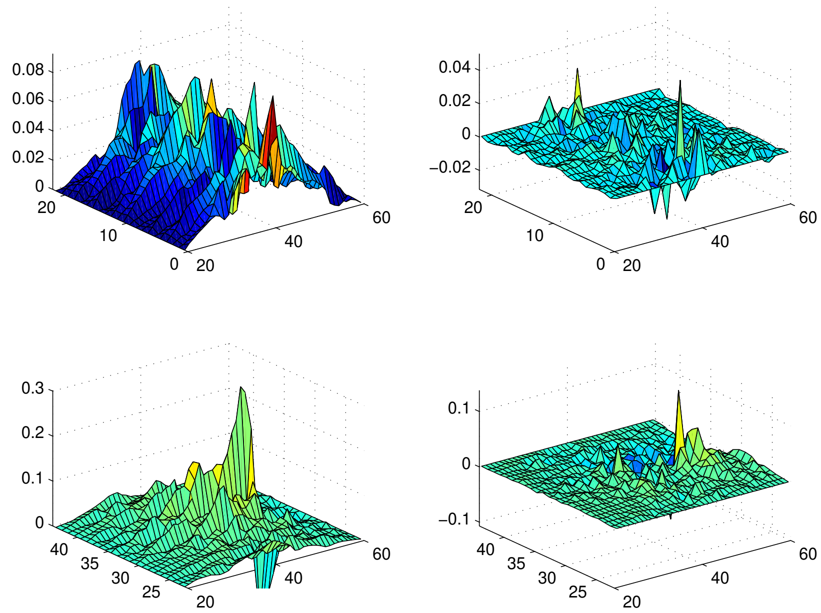

Fig. 2.3. *The x-component (left) and y-component (right) of two MMsFEM base functions for a two dimensional model with random coefficients. The top base function corresponds to an interface away from the near well region and is constructed using (2.10) while the bottom base function corresponds to a well block interface and is constructed using (2.11).*

We also mention that Chen and Yue, [12], have used a similar type of technique to deal with wells using a Galerkin MsFEM with oversampling. Their work seems to be pioneering in the direction of mathematically rigorous treatment of wells in reservoir simulation, but the MsFEM itself is not mass conservative. Neither would it be mass conservative if they did not use an oversampling strategy because the method is based on the Galerkin version of the MsFEM, [19]. However, the new developments that they propose with respect to well treatment can easily be invoked into the construction of the MMsFEM base functions (2.5)-(2.6). Though we believe that this will not have a strong impact on the accuracy of our method, their analysis could be useful for proving theoretical convergence estimates for the proposed MMsFEM in the case of periodic coefficients using homogenization theory.

One of the main improvements in the modified MMsFEM as compared with reservoir simulation schemes based on upscaling is perhaps that we have included a more flexible treatment of the wells that allows us to model the wells at the subgrid level using e.g., the numerical well-models proposed by Chen and Yue in [12]. Moreover, in both the static and dynamic approach we can easily define base functions that correspond to arbitrary well configurations as long as these can be correctly modeled at the subgrid scale. Hence, the new MMsFEM also offers the possibility of running reservoir simulations with complex well-architectures without resorting to somewhat ad-hoc near-well upscaling procedures. Since it is well known that capturing the flow behavior in the vicinity of the wells is of great importance in order to obtain an accurate flow scenario, we believe that the modified MMsFEM provides a step toward a more robust and rigorous treatment of wells in reservoir simulation.

3. Discretization of the saturation equation. The most common reservoir simulation schemes use an implicit pressure explicit saturation (IMPES) strategy to decouple the governing equations (1.4), (1.6). That is, the pressure is computed at the current time-step with mobility coefficients defined with saturation values from the previous time-step. The saturation equation is then solved with an explicit Euler method using pressure values from the previous time-step and with the gravitational mobility calculated with saturation values from the previous time-step. This strategy will also be employed here. Hence, after solving the elliptic pressure equation (1.4) and generating the respective velocity fields, we discretize the saturation equation with a standard upstream-weighted finite volume method:

$$S_i^{k+1} = S_i^k + \frac{\Delta t}{\phi_i |V_i|}\left(Q_i(S^k) - \sum_{j\neq i} V_{ij}(S^k)(v_{ij} + g_{ij}(S^k))\right) . \tag{3.1}$$

Here Δt denotes the time step, ϕ_i is the porosity in the grid cell V_i and $|V_i|$ is the measure of V_i. Furthermore, $Q_i(S) = \int_{V_i} q_w(S)$ is the source term contribution in V_i and $V_{ij}(S) = \max\{sign(v_{ij})f_w(S_i), -sign(v_{ij})f_w(S_j)\}$ is the upstream weighted fractional flow function for $\gamma_{ij} = \partial V_i \cap \partial V_j$. Finally,

$$v_{ij} = -\int_{\gamma_{ij}} K\lambda_t \nabla p \cdot n_{ij}\, ds \quad \text{and} \quad g_{ij}(S) = \int_{\gamma_{ij}} K\lambda_o(\rho_w - \rho_o)G \cdot n_{ij}\, ds\ ,$$

where n_{ij} is the unit normal to γ_{ij} pointing from V_i to V_j.

4. Numerical results. The purpose of this section is to assess the accuracy of the production scenarios induced by the MMsFEM as compared with reference production scenarios obtained by solving the pressure equation (1.4) at the subgrid level. In both cases the saturation equation (1.6) is solved at the subgrid level using the upstream weighted finite volume method (3.1). The qualitative measure is a plot of the respective water-cut curves, that is curves showing the fraction of water in the produced fluid as a function of time.

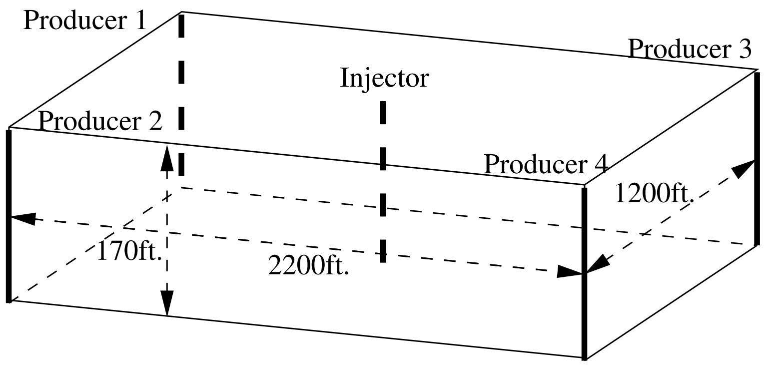

FIG. 4.1. *The figure depicts the reservoir domain with a producer at each corner and an injector at the center. The grid dimensions are* $1200 \times 2200 \times 170$ *feet. The fine grid numerical model consists of* $30 \times 110 \times 17$ *equally sized cells of size* $40 \times 20 \times 10$ *feet and the wells perforate all layers.*

A schematic of the reservoir domain is shown in Figure 4.1. The permeability field consists of two separate heterogeneous formations that are sampled from an upscaled version of the SPE comparative solution project, model 2, [10]. The top

70 ft (7 layers) represent the Tarbert formation and the bottom 100 ft (10 layers) represent the Upper Ness formation. We have plotted the logarithm of the average of the permeability layers in the Tarbert and Upper Ness formations in Figure 4.2. We observe that the permeability map that corresponds to the Tarbert formation appears to be much smoother than the permeability distribution in the Upper Ness formation.

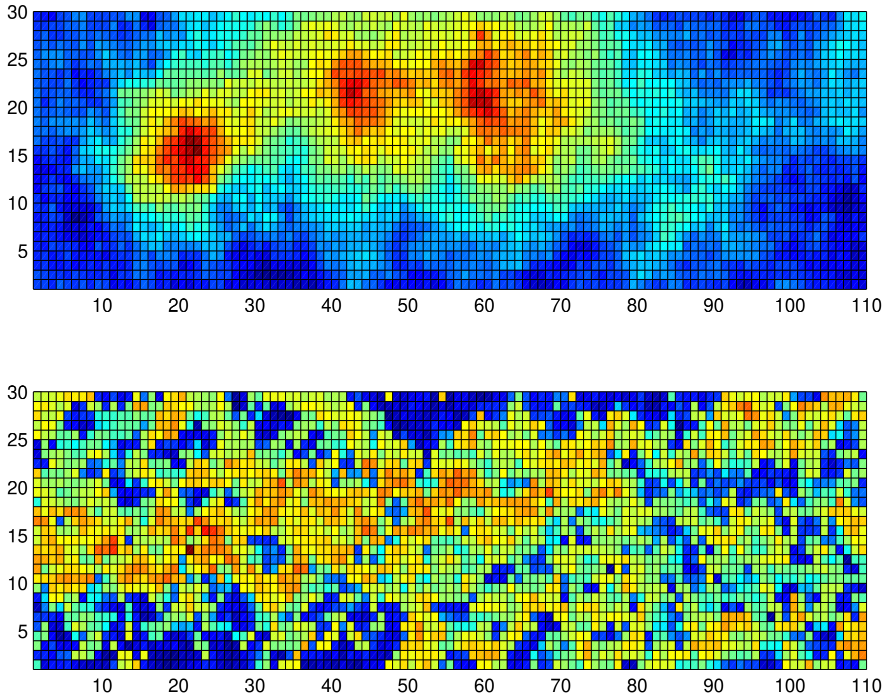

FIG. 4.2. *The figure illustrates the heterogeneous structures in the Tarbert formation (top) and the Upper Ness formation (bottom) that was used in the SPE 10th comparative solution project.*

In our test cases we have not included the variability in the porosity, and use $\phi = 0.2$ in the entire reservoir. The mobility functions are defined to be

$$\lambda_w(S) = c\left(\frac{S - S_{rw}}{1 - S_{rw} - S_{ro}}\right)^j \quad \text{and} \quad \lambda_o(S) = \left(\frac{1 - S - S_{ro}}{1 - S_{rw} - S_{ro}}\right)^j \tag{4.1}$$

where $S_{rw} = S_{ro} = 0.2$ are the residual oil and water saturations. Here c is a free parameter that we shall use to obtain different flow conditions. Finally, the initial condition is $S(x, 0) \equiv S_{rw}$ and we inject 5000 barrels of water per day. The total production rates for each producer are all equal to one fourth of the injection rate.

4.1. Steady-state two-phase flow. If we neglect gravity and set $c = j = 1$ in (4.1), then λ_t will not depend on saturation and we obtain a steady state situation. This implies that the pressure equation (1.4) needs to be solved only once and that the Darcy velocity field v will be constant in time. Steady-state conditions can therefore be used illustrate the impact of errors in a fixed velocity field. For the steady state simulations below we have only employed the static method for determining local boundary conditions. We compare the induced water-cut curves with those obtained from a reference solution where we solve the pressure equation at the subgrid level.

We also compare the MMsFEM water-cut curves with the water-cut curves obtained using the nested gridding approach proposed by Gautier et al., [17]. In this method a subgrid velocity field is obtained as follows. First the elliptic equation is solved at the coarse scale level using the upscaling procedure proposed by Durlofsky, [14][1]. We then recover the subgrid velocity field from the coarse scale fluxes in the same way as we do in the MMsFEM. Thus we use the same well-model and the same considerations to anticipate the local variations in the flow velocity at the block interfaces. Hence, the only difference between the nested gridding technique that we use here and the proposed MMsFEM is that we use a different method to determine the coarse grid fluxes. The methods have about the same complexity since the upscaling procedure [14] require that we solve three subgrid problems analogous to (2.5)-(2.6) for each coarse grid block in order to determine the upscaled permeability tensors.

Instead of running simulations with the Tarbert formation on top of the Upper Ness formation as was done in the 10th SPE comparative solution project, we run separate simulations with each of the two geological formations. This is because the permeability distributions in the Tarbert formation and in the Upper Ness formation are qualitatively different. Though the permeability in both formations span over more than eight orders of magnitude, the permeability distribution in the Tarbert formation is smoother and hence much easier to upscale.

Figure 4.3 show the water-cut curves for the respective steady-state simulations over the Tarbert and Upper Ness geological formations. Table 4.1 quantifies the discrepancy between the water-cut curves ω_{wc} in the relative norm

$$e(\omega_{wc}) = \frac{\|\omega_{wc} - \omega_{wc}^{ref}\|}{\|\omega_{wc}^{ref}\|}\ , \tag{4.2}$$

where ω_{wc}^{ref} is the reference water-cut curve. We see that both the MMsFEM and the nested gridding technique produce accurate production scenarios for the Tarbert formation. For the Upper Ness formation the MMsFEM gives a good match with the reference water-cut curves associated with producer 1-3, but not so good for producer 4. However, it performs consistently better than the nested gridding technique.

The discrepancy that we see between the reference water-cut curves and the ones induced by the MMsFEM can be explained by the use of improper boundary conditions. Indeed, if we had chosen exact boundary conditions then we would have had an exact match between the water-cut curves. The nested gridding technique does not have this kind of property since it relies on an intermediate upscaling step. This favorable property inherent in the MMsFEM will become clearer as we consider dynamic flow conditions in the next section. We will there employ the alternative dynamic strategy for determining local boundary conditions.

4.2. Dynamic two-phase flow. We now include gravity and set $j = 2$ in (4.1) so that λ_t becomes a dynamic function of the saturation S_w. This means that we now have to update the Darcy velocity field throughout the simulation. The impact of the dynamic coupling between (1.4) and (1.6) on the flow scenario depends on the mobility ratio, i.e., on the aspect ratio of the extremal values for λ_t. Thus, while it may be sufficient to use a fixed set of base functions for two-phase flow simulations with a low mobility ratio, a high mobility ratio may indicate that we need to regenerate some of the MMsFEM base functions during the simulation.

[1]This method is one of the most popular and most robust upscaling techniques for steady state flow simulations.

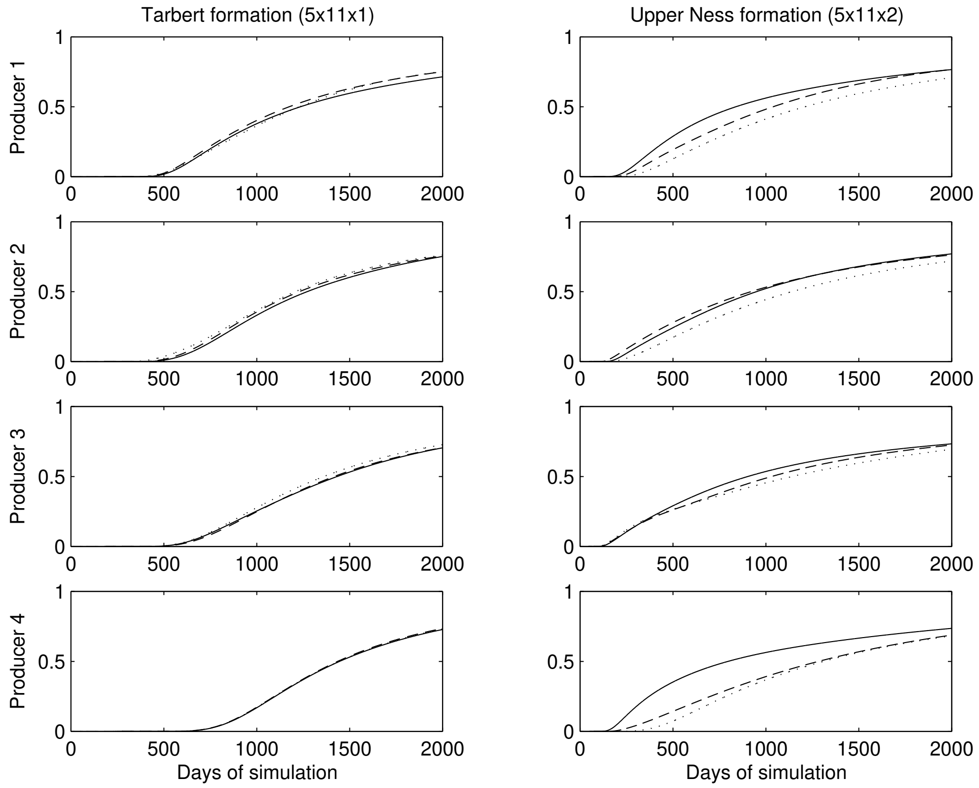

FIG. 4.3. *Water-cut curves induced by a velocity field generated by the MMsFEM (dashed line), the reference solution (solid line) and the nested gridding technique (dotted line) respectively. The figures to the left show the water-cut curves for the Tarbert formation and the figures to the right show the water-cut curves for the Upper Ness formation. The coarse grid dimensions are respectively* $5 \times 11 \times 1$ *for the Tarbert formation and* $5 \times 11 \times 2$ *for the Upper Ness formation.*

$e(\omega_{wc})$	Tarbert formation		Upper Ness formation	
Producer	MMsFEM	Nested Gridding	MMsFEM	Nested Gridding
1	.044	.038	.075	.144
2	.022	.040	.024	.087
3	.008	.036	.040	.073
4	.008	.005	.174	.211

TABLE 4.1
The table shows relative discrepancy $e(\omega_{wc})$ *between the water-cut curves induced by the MMsFEM and the nested gridding technique and the water-cut curves induced by the reference solution.*

In this section we define the boundary conditions for $\hat{p}$ and the base functions in the "dynamic" way (2.13)-(2.14). We will further use the adaptive criteria (2.9) to illustrate that good results can be obtained by recomputing a small portion of the base functions for each time step. We first consider three test cases defined by three different values of c in (4.1), one case with a mobility ratio of 2 ($c = 1$) and two cases with a mobility ratio of 5 ($c = 1/4$ and $c = 4$). For all three cases we run simulations using three different values of the adaptive selection threshold: $C = 0$, $C = 1/4$ and $C = 4$. These threshold values correspond to regenerating all, roughly $\sim 5\%$, and none of the base functions for each time step. Hence, setting $C = 4$ implies that we use a fixed set of base functions defined by (2.13)-(2.14) with $t = t_0$ throughout the simulation. We wish to emphasize that the induced subgrid velocity field will be mass conservative either we regenerate the base functions or not. This follows from the definition of the base functions (2.5)-(2.6) and equation (2.2).

We only run simulations over the Upper Ness formation since the steady-state simulations in §4.1 showed that this formation contained the difficult heterogeneous structures. The coarse grid dimensions are $5 \times 11 \times 2$. Figure 4.4 shows the water-cut curves induced by the reference solution and by the MMsFEM for the three adaptive selection threshold values. Table 4.2 quantifies the discrepancy between the water-cut curves induced by the MMsFEM and those induced by the reference solution in the relative norm (4.2).

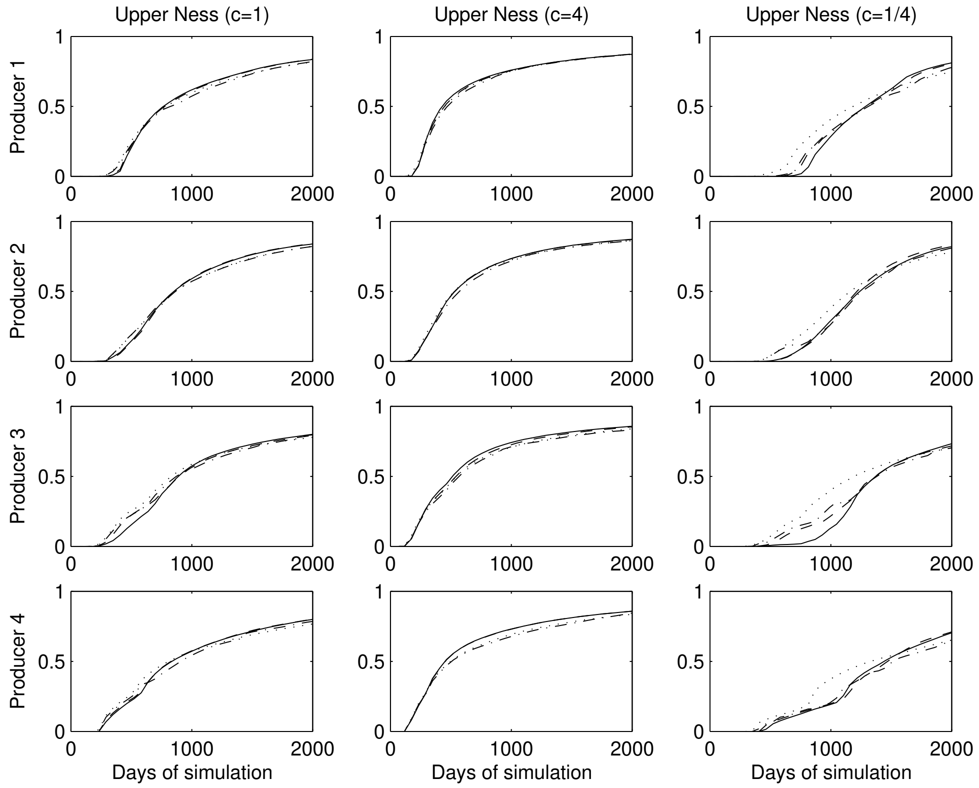

FIG. 4.4. *The figure depicts the water-cut curves produced by the reference two-phase flow simulation (solid line) over the Upper Ness formation for three different sets of mobility functions λ_o and λ_w and by the MMsFEM simulations with the same mobility functions and three different values of the adaptive selection parameter C. The dashed line corresponds to $C = 0$, the dash-dot line corresponds to $C = 1/4$ and the dotted line corresponds to $C = 4$.*

The results in Figure 4.4 and Table 4.2 show that the process of determining local boundary conditions with the aid of the initial flow velocity v^0 gives much better results than the static approach used for the steady-state simulations in §4.1. Indeed, if we regenerate the base functions for each time step using the boundary conditions defined by (2.13)-(2.14), then we see that we get a very good match with the reference water-cut curves in practically all the situations considered. We also see

$e(\omega_{wc})$	$c=1$			$c=4$			$c=1/4$		
Prod	C=0	C=$\frac{1}{4}$	C=4	C=0	C=$\frac{1}{4}$	C=4	C=0	C=$\frac{1}{4}$	C=4
1	.007	.032	.029	.008	.020	.011	.035	.054	.107
2	.006	.028	.025	.002	.017	.013	.020	.030	.072
3	.031	.042	.060	.015	.036	.024	.067	.098	.186
4	.006	.034	.046	.001	.041	.029	.022	.056	.121

TABLE 4.2

The table shows the discrepancy between the water-cut curves induced by the MMsFEM for three different set of mobility functions λ_o and λ_w and three different values of the adaptive selection parameter C and the water-cut curves induced by the corresponding reference solution.

that using a fixed set of base functions gives good results for both $c = 1$ and $c = 4$. The intermediate threshold value, $C = 1/4$, which identified roughly 5% of the base functions at each time step, produced overall good results. For instance, for $c = 1/4$ the errors in Table 4.2 corresponding to $C = 1/4$ are about half the size of the errors corresponding to $C = 4$.

We observe that even though the mobility ratio is the same for $c = 4$ and $c = 1/4$, the latter case produced larger errors. This indicates that the mobility ratio alone is not enough to identify flow conditions that require the base functions to be updated during the simulation. Indeed, the flow pattern induced by $c = 4$ is qualitatively different from the flow pattern induced by $c = 1/4$ as Figure 4.5 shows.

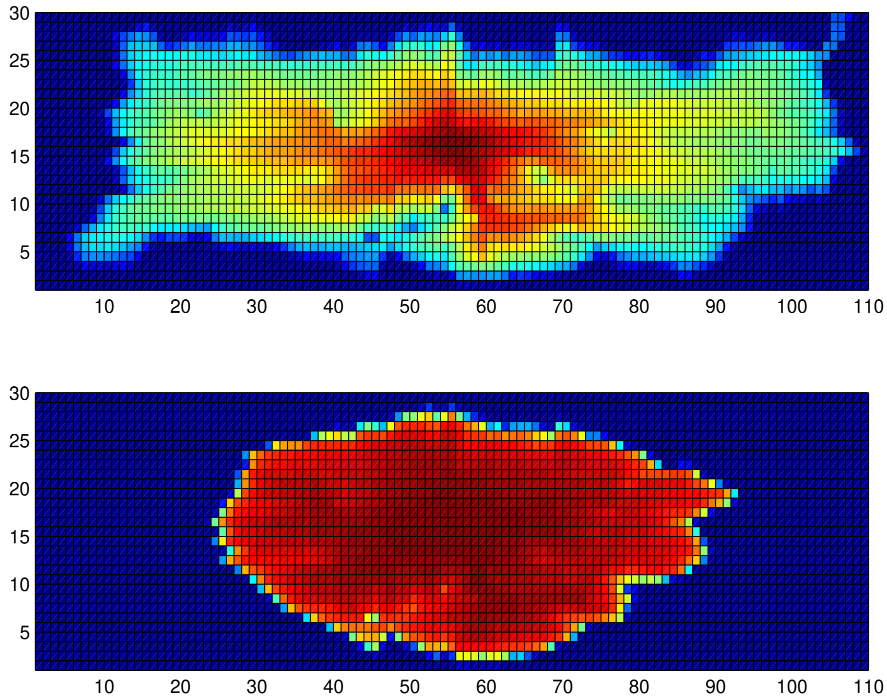

FIG. 4.5. *Saturation profiles (computed with the reference simulation scheme) for $c = 4$ (top) and $c = 1/4$ (bottom) after 20% of the total accecible pore volume in the reservoir has been injected (~ 640 simulation days). The reservoir domain is here a plane region with a permeability distribution equal to the average of the permeability layers in the Upper Ness formation.*

For $c = 4$ the water-phase have superior flow properties to the oil-phase. This causes a pistol-like displacement process which creates a low saturated zone that moves quickly toward the producers. This, leads to a rather smooth saturation profile that produces a slowly varying total mobility function. In particular, we seldom see large variations in the total mobility inside a coarse grid block. Hence, assuming e.g., constant mobility when constructing the MMsFEM base functions will in general give adequately accurate velocity fields throughout the simulation.

For $c = 1/4$, on the other hand, the water-phase tends hesitate to displace the oil-phase and produces a very sharp displacement front. This, in turn, induces large gradients in the total mobility near the saturation front. Thus, in the latter case it becomes important to capture the fine scale characteristics at the interface between the two phases. This implies that we need to regenerate the base functions in regions where the saturation profile exhibits large gradients.

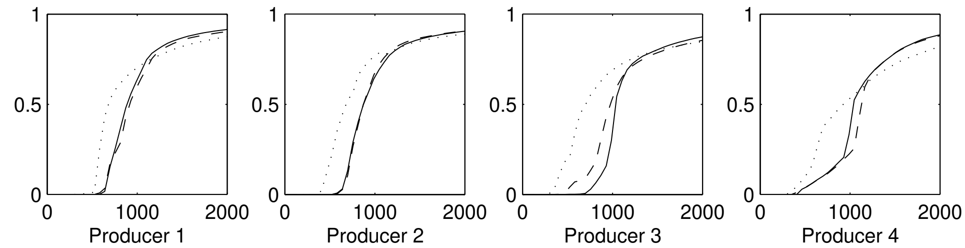

FIG. 4.6. *The figure shows the water-cut curves produced by the reference solution (solid-line) and the MMsFEM with $C = 0$ (dashed line) and $C = 4$ (dotted line) with $c = 1$ and $j = 4$ in (4.1).*

A similar situation occurs if we set $c = 1$ and $j = 4$ in (4.1). This is seen in Figure 4.6 where we see that there is large discrepancy between the reference water-cut curve and the water-cut curve produced using the MMsFEM with a fixed set of base functions. In this case we also have a sharp displacement front that is caused by the sharp transition in the fractional flow curves, i.e., the fractional flow function is very flat for values of the saturation below a certain threshold value. This type of sharp transition is also present in the fractional flow curve that corresponds to setting $c = 1/4$ and $j = 2$ in (4.1), but not in the fractional flow curve that corresponds to setting $c = 4$ and $j = 2$ in (4.1). Thus, while the simple adaptive selection criteria (2.9) appears to be a valid measure for when the base functions need to be updated, the shape of the fractional flow function f_w might be a better indicator than a high mobility ratio in terms of determining what kind of flow conditions that require that we regenerate the MMsFEM base functions during the simulation.

5. Concluding remarks. We have made an attempt to show that the mixed multiscale FEM can be a valuable tool in reservoir simulation, both as a measure to simplify the numerical treatment (more flexibility in the grid generation and less need for upscaling procedures) and as a tool to, either obtain coarse grid solutions with higher accuracy or fine grid solutions with less computation time. With these objectives in mind, we have modified the original mixed multiscale FEM of Chen and Hou, [11], in order to improve the treatment of wells and to produce a velocity field which can be used to simulate the phase transport at the subgrid-scale.

The proposed mixed multiscale FEM has in general showed a very good ability to capture the effect of the subgrid heterogeneous structures, and hence to predict accurate production scenarios. For steady-state flow conditions we considered a deterministic approach to specifying boundary conditions for the mixed multiscale FEM base functions. This proved to work well, but there were some notable discrepancies with the reference water-cut curves when we simulated with the difficult heterogeneous structures in the Upper Ness formation. Nevertheless, the mixed multiscale FEM performed consistently better than the nested gridding technique, [17].

For the dynamic two-phase flow simulations we used an alternative dynamic approach to determine the boundary condition for the base functions where we extract information about the global flow pattern from the initial velocity field. This approach proved to work remarkably well in the sense that if we regenerate the base functions for each time step, then we obtain a very good match with the reference production scenarios. We also investigated what kind of mobility functions induce flow conditions that require that we regenerate the base functions during the simulation, and showed that it is possible to determine a selection criteria for identifying which of the base functions that need to be recomputed for each update of the total velocity field.

In this paper we have focused on incompressible two-phase flow. Hence, a step for future work is to approach compressible three-phase flow simulation. Of coarse, there are many more issues that may be addressed, but the main message here is (i): the multiscale FEM's are not as complex as they may seem, (ii): they provide a robust alternative to upscaling and a step in the direction of routine reservoir simulations on desktop computers, and (iii): they simplify the numerical treatment of wells in reservoir simulation, especially when the wells have complex well architectures. As complex non-conventional wells are becoming increasingly popular in the oil-industry, the specific use of the mixed multiscale FEM as a tool to handle such wells could also be a natural topic for future work.

Acknowledgments: I wish to thank Knut-Andreas Lie and the anonymous referees for valuable feedback that helped improve the quality of the paper.

REFERENCES

[1] I. Babuška, G. Caloz, E. Osborn, *Special finite element methods for a class of elliptic problems with rough coefficients* SIAM J. Numer. Anal., 31(1994): pp. 945-981.

[2] I. Babuška, E. Osborn, *Generalized finite element methods: Their performance and their relation to mixed methods*, SIAM J. Numer. Anal., 20(1983): pp. 510-536.

[3] J.W. Barker, S. Thibeau, *A critical review of the use of pseudorelative permeabilities for upscaling*, SPE Reservoir Eng. 35491, 12(1997): pp. 138-143.

[4] I. Berre, H.K. Dahle, K.H. Karlsen, H.F. Nordhaug, *A streamline front-tracking method for two- and three-phase flow including capillary forces*, Contemp. Math., Z. Chen, R.E. Ewing eds., AMS, Providence, Rhode Island, 295(2002): pp. 49-61.

[5] D. Braess, *Finite elements: Theory fast solvers and applications in solid mechanics*, Cambridge University Press, Cambridge, 1997.

[6] F. Bratvedt, T. Gimse, C. Tegnander, *Streamline computation for porous media flow including gravity*, Transp. Porous Media, 25(1996): pp. 62-78.

[7] S.C. Brenner, L.R. Scott, *The mathematical theory of finite element methods*, Springer-Verlag, New-York, 1994.

[8] F. Brezzi, M. Fortin, *Mixed and hybrid finite element methods*, Computational Mathematics, Springer-Verlag, New-York, 1991.

[9] M.A. Christie, *Upscaling for reservoir simulation*, JPT J. Pet. Tech., 48(1996): pp. 1004-1010.

[10] M.A. Christie, M.J. Blunt, *Tenth SPE comparative solution project: A comparison of upscaling techniques*, SPE 72469, 2001. Website: www.spe.org/csp

[11] Z. Chen, T.Y. Hou, *A mixed multiscale finite element method for elliptic problems with oscillating coefficients*, Math. Comp., 72(2003): pp. 541-576.

[12] Z. Chen, X. Yue, *Numerical homogenization of well singularities in the flow transport through heterogeneous porous media*, SIAM Multiscale Model. Simul., Vol 1, 2(2003): 260-303.

[13] A. Desbarats, *Spatial averaging of hydraulic conductivity under radial flow conditions*, Math. Geol., 1994: pp. 1-21.
[14] L.J. Durlofsky, *Numerical calculations of equivalent gridblock permeability tensors for heterogeneous porous media*, Water Resour. Res., Vol. 27, 5(1991): pp. 699-708.
[15] L.J. Durlofsky, *Scale-up in the near-well region*, SPEJ. 2000: pp. 110-117.
[16] L.J. Durlofsky, R.C. Jones, W.J. Milliken, *A nonuniform coarsening approach for the scale-up displacement processes in heterogeneous porous media*, Adv. Water Res., Vol 20, 5-6(1997): 335-347.
[17] Y. Gautier, M.J. Blunt, M.A. Christie, *Nested gridding and streamline based simulation for fast reservoir performance prediction*, SPE 51931, 1999.
[18] U. Hornung, *Homogenization and porous media*, Springer-Verlag, New-York, 1997.
[19] T.Y. Hou, X-H Wu, *A multiscale finite element method for elliptic problems in composite materials and porous media*, J. Comput. Phys., 134(1997): pp. 169-189.
[20] P. Jenny, S.H. Lee, H.A. Tchelepi, *Multi-scale finite-volume method for elliptic problems in subsurface flow simulation*, J. Comput. Phys., 187(2003): pp. 47-67.
[21] V.V. Jikov, S.M. Kozlov, O.A. Oleinik, *Homogenization of differential operators and integral functionals*, Springer-Verlag, New-York, 1994.
[22] J.R. Kyte, D.W. Berry, *New pseudofunctions to control numerical dispersion*, SPEJ 5105, (1975): pp. 269-276.
[23] D.W. Pollock, *Semianalytical computation of path lines for finite difference models*, Ground Water, Vol. 26, 6(1988): pp. 743-750.
[24] P. Renard, G. de Marsily, *Calculating equivalent permeability: A review*, Adv. in Water Resour., 20(1997): pp. 253-278.
[25] H.L. Stone, *Rigorous black-oil pseudofunctions*, SPE 21207, 1991.
[26] X.-H. Wen, J.J. Gómez-Hernández, *Upscaling hydraulic conductivities in heterogeneous media: An overview*, J. Hydrol., 183(1996): pp. ix-xxxii.